EFFECT OF SINTERING ON STRUCTURAL AND MAGNETIC PROPERTIES OF MANGANESE FERRITE NANOPARTICLES

Submitted in partial fulfilment of the requirement for the award of the

Degree of

MASTER OF SCIENCE

In

PHYSICS

Submitted by

YASHPREET
(ROLL No. 301504041)

Under the supervision of

Dr. B.N. CHUDASAMA
Associate Professor

School of Physics and Material Science
Thapar University, Patiala
Punjab-147004

July - 2017

Dedicated to my family

CERTIFICATE

This is to certify that **Ms. YASHPREET**, Roll No. **301504041** has worked on this thesis report entitled **"EFFECT OF SINTERING ON STRUCTURAL AND MAGNETIC PROPERTIES OF MANGANESE FERRITE NANOPARTICLES"** in partial fulfilment for the award of the degree of MASTER OF SCIENCE in PHYSICS in THAPAR UNIVERSITY, PATIALA was carried out by her under my supervision. She has not submitted this material for credit towards any other degree at Thapar University, Patiala or any other University.

(Dr. B. N. Chudasama)
Associate Professor
School of Physics and Materials Science
Thapar University, Patiala

i

ACKNOWLEDGEMENT

This Research work was carried out during the Session 2015-2017 at the School of Physics and Materials Science in Thapar University, Patiala.

I owe my deepest gratitude to my supervisor Dr. B. N. Chudasama Associate Professor, School of Physics and Materials Science in Thapar University, Patiala, for his valuable guidance, constant encouragement during my research work encouragement and support this study would hardly have been completed. He is always willing to listen, discuss and advice throughout the work. His support and inspiring suggestions have been precious for the development of this thesis content.

I am deeply grateful to Dr. Manoj Sharma, Professor and Head, School of Physics and Material Science, for his support and for providing me infrastructural facilities to conduct this research work.

I would like to thank Mrs. Parveer Kaur, Ms. Navjot Kaur, Ms. Poornima, research scholars for the help provided by them in lab. This dissertation would not have been possible without their support and discussions.

I owe more than thanks to my family for their support and encouragement throughout my life. Words cannot express how grateful I am to my mother for their love, prayers, caring and sacrifices for educating and preparing me for my future. Finally, I thank almighty God for giving me power to follow the right direction in achievement of my goal.

Yashpreet.

Ms. YASHPREET

ii

ABSTRACT

Sintering is an essential step used in most of the synthesis processes. Magnetic nanoparticles are synthesized by variant of methods and in most of the cases they are subject to sintering to improve specific characteristics like hardness or magnetization. Co-precipitation is a very popular and easy technique to synthesize various nanoparticles, especially ferrites. Manganese ferrite nanoparticles are routinely synthesized by chemical coprecipitation technique. Effect of sintering on the structural and magnetic properties of manganese ferrite nanoparticles synthesized by coprecipitation method is not well understood. In this dissertation, effect of sintering on structural and magnetic properties of manganese ferrite nanoparticles has been studied. When sintered at 400 °C, as-synthesized $MnFe_2O_4$ nanoparticles decompose into γ-Fe_2O_3 and Mn_3O_4. Upon further heating at 600 °C, γ-Fe_2O_3 gets transformed into α-Fe_2O_3. When $MnFe_2O_4$ is sintered at 900 °C, it decomposes into three crystallographic phases, i.e. α-Fe_2O_3, Mn_3O_4 and Fe_3O_4. The corresponding changes in the magnetic properties are in good agreement with the observed changes in the structural properties of the $MnFe_2O_4$ due to sintering.

CONTENTS **PAGE NO.**

LIST OF FIGURES PAGE NO.

LIST OF TABLES PAGE NO.

CHAPTER 1 INTRODUCTION

1.1. Nanoscience and Nanotechnology

The most widely recognized working meaning of Nanoscience will be: “Nanoscience is the study of phenomena and manipulation of materials at micro and macromolecular scale, in which properties vary notably from the ones at bulk scale” [1].

The macroscopic or bulk materials have continuous physical properties. When the particles are at nanoscale dimensions, the classical physics principles have no longer accomplished for designating their behaviour. But at this dimensions the quantum physics principles apply. The properties of material such as gold at the nano scale shows different as compared to macro scale. Colour, electrical conductivity, and strength of material are those properties which changes while its size reduces to nano scale.

“Nanotechnology is the characterisation, design, production and application of structures, devices and systems by controlling the size and shape at nano scale.” The word nano originates from the Greek word nano that means very small particles [2]. Hence, nanoscience and nanotechnologies deals with at least groups of particles of 1 nm in length (Figure 1.1).

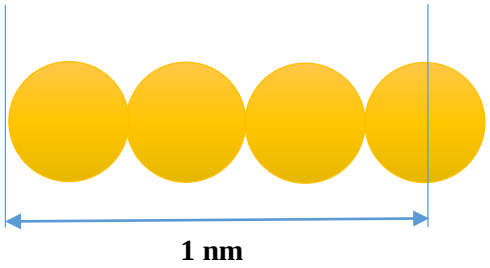

Figure 1.1. Set of Three and a Half gold particles in progression identical to length of 1 nm.

Nanoscience is not just the science of dimension in the range of “1 to 100 nm” of certain material which centres on the dimension effects, but a science of new physical phenomena shows in the material with the small dimensions, this effect is collectively named as quantum effects, that dependent on the size and intensely different from macro-scale materials properties.

Nanoparticles are bigger than one particular atom but slighter than the cells and bacteria. It is beneficial to practice a scale similar to the one which is shown in figure 1.2 where we can imagine the connection between the bulk materials, as tennis ball, and the nanomaterial's [1].

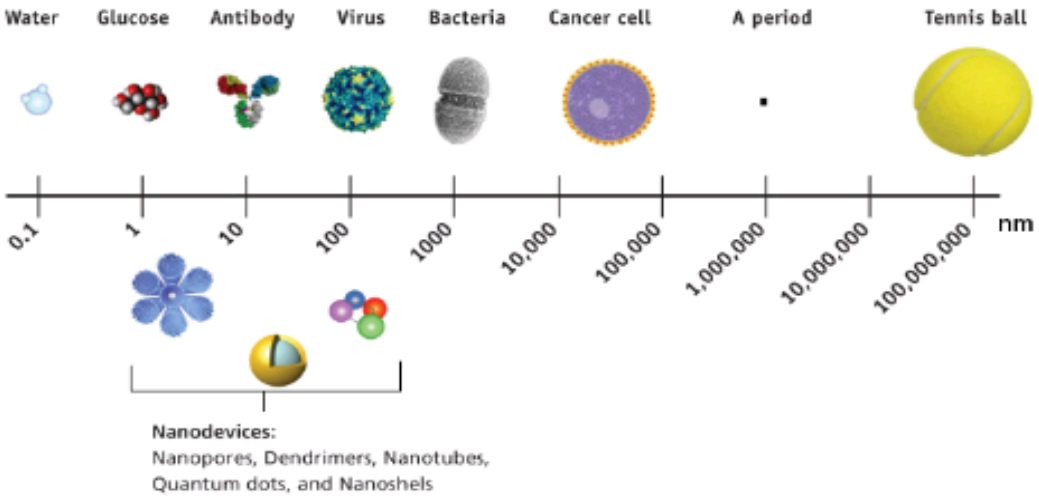

Figure 1.2. Transformation of macro-materials to nano-materials through a scale [1].

1.2. Effect of size on magnetic properties

The magnetic properties at nano scale are quite different from the bulk particles. The properties of magnetic nanoparticles are changed from bulk because of the surface effects. Saturation magnetization of Ferromagnetic materials decrease correspondingly with reduction of size in magnetic materials due to surface effects [3]. The value of saturation magnetization with the change in particle size of Fe_3O_4 (spherical magnetite) is shown in figure 1.3. The saturation magnetization decreases with reduction in the particle size [3].

The coercivity, remanence and Curie temperature (T_c) is decreases as the particle size decreases from bulk to nano scale [5]. Anisotropy of the magnetic structures which increases from the bulk to nano scale [4].

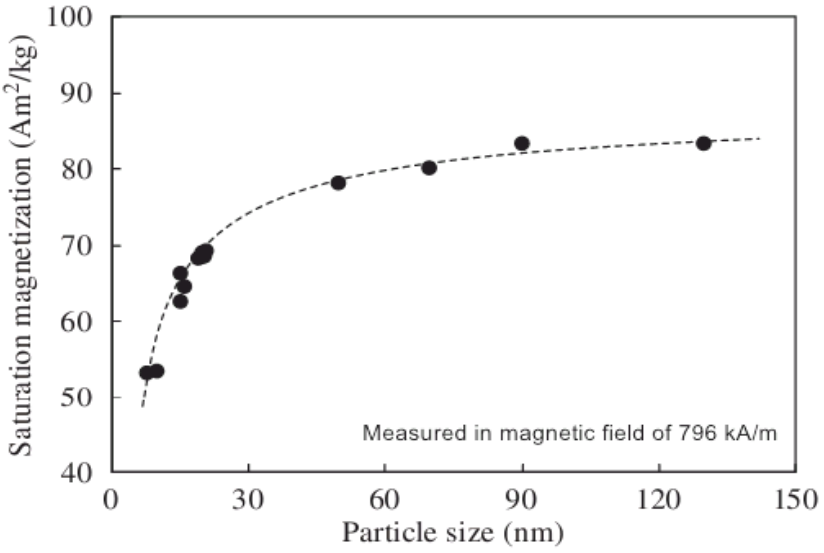

Figure 1.3. The value of saturation magnetization (M_s) with the change in particle size of Fe_3O_4 [3].

1.3. Ferrites

Ferrites are ceramic composites which contains iron oxide and other metals [6]. M^{2+} O $Fe^{3+}{}_2$ O_3 is the molecular formula of ferrites in which M denotes the divalent metal like Fe, Co, Mn, Ni, Mg, Cd, Cu, Zn. 8 molecules per unit cell are arranged in a spinel structure. Ferrites are called as metal oxide that encloses magnetic ions which grouped together in such a way that it creates spontaneous magnetization [7]. Ferrites gives us low eddy current and dielectric losses, reasonable permittivity, and high value of magnetic permeability, electrical resistivity, saturation magnetization, and Curie temperature which confirms that it is a good insulating magnetic material [8]. With the presence of these properties ferrites are used in various applications. The other applications of ferrites are that they are used in magnetic recording media, permanent magnets, memory chips, transformer cores, antenna rods, and in computer technology [9]. They could be used in magnetic resonance imaging, drug delivery, gas sensors, actuators, and also in magnetic fluids [10].

1.4. Classification of Ferrites

Ferrites are divided into two type’s namely soft and hard ferrites.

1.4.1. Soft ferrites

Soft ferrites have low coercivity, high saturation magnetization, low remanent magnetization, and low eddy current losses. They also have high value of susceptibility and permeability. Soft ferrite are not appropriate for permanent magnets because they are easily demagnetized and magnetized. The B-H loop of the soft ferrites are narrow (Figure 1.4). Iron, cobalt and manganese are the examples of soft ferrites.

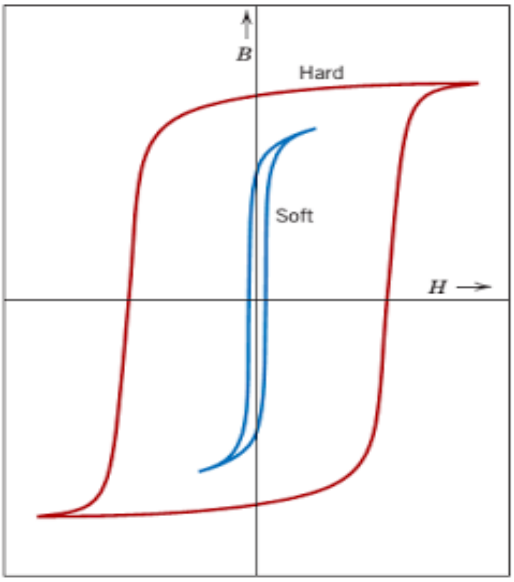

Figure 1.4. Comparison between soft and hard ferrite from the hysteresis loop.

They are used to make ferrite core for inductor and transformer in electronic industry and also used to make the components of microwave [11, 12]. Manganese-zinc, Nickel-zinc ferrite are the most common soft ferrites.

1.4.2. Hard ferrites

Hard ferrites have high coercivity, low saturation magnetization, and high remanent magnetization. They are used for making permanent magnets because they are difficult to demagnetize and magnetize. It is tough to demagnetize a material when it is magnetize in a field. The B-H loop of the hard ferrites are broad as compared to soft ferrites (Figure 1.4). They are used to make permanent magnets. They are also used in loudspeakers, electric motors,

refrigerators, automobiles, air crafts, etc. [11, 12]. Strontium ferrite, Cobalt ferrite, and Barium ferrite are the various examples of hard ferrite.

1.5. Structure of ferrites

1.5.1. Normal Spinel

When the octahedral [B] sites are occupied by the one kind of cations then the spinel is named as the normal spinel. In these type of ferrites, the divalent cation are poisoned at tetrahedral [A] site while the trivalent cation are positioned at octahedral site [B]. The formula of the Normal spinel is given as $M^{2+}\,M^{3+}{}_2\,O_4$ and here M^{2+} is represented as the divalent metal e.g. manganese that occupy the tetrahedral [A] sites and M^{3+} is represented as the trivalent metal e.g. iron that occupy the octahedral [B] sites [13].

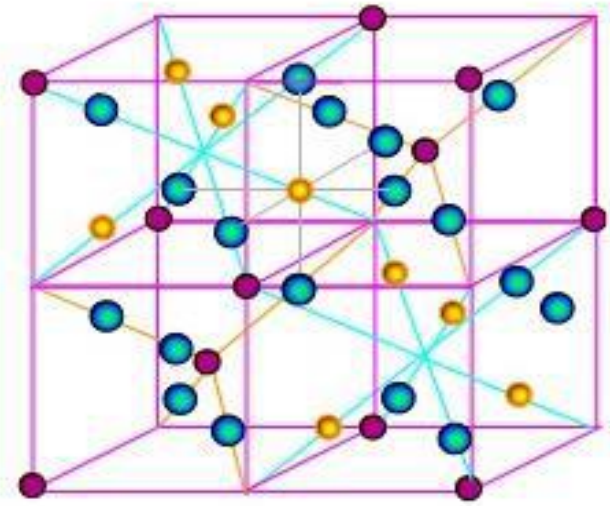

Figure 1.5. Normal spinel ferrites structure in which manganese are represented by the purple, iron by the yellow, and oxygen by the blue atoms.

1.5.2. Inverse spinel

Where half of the trivalent ions are positioned at the tetrahedral [A] sites and the other half of the trivalent and divalent ions are positioned at the octahedral [B] sites. The formula for the inverse spinel ferrite structure is represented as $M^{3+}M^{2+}M^{3+}O_4$, and here M^{2+} is represented as divalent metal e.g. manganese that occupy the octahedral [B] sites and M^{3+} is trivalent metal e.g. iron that equally occupy the tetrahedral [A] and octahedral [B] sites [14, 15].

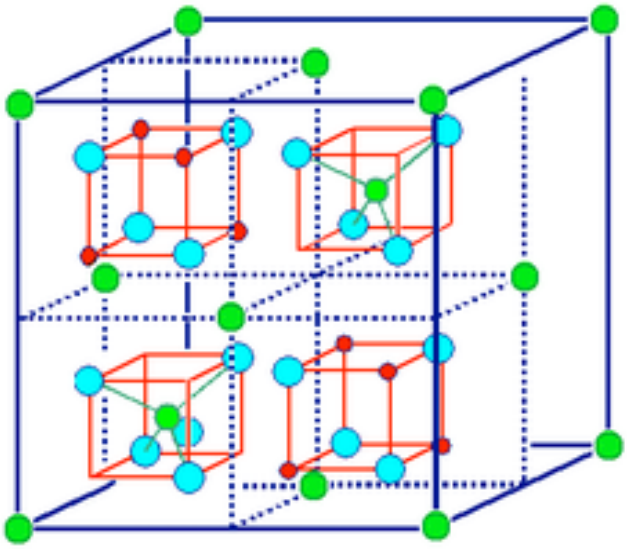

Figure 1.6. Crystal structure of inverse spinel ferrites.

1.5.3. Intermediate Spinel

These structures are also termed as random spinel. In between the tetrahedral [A] and the octahedral [B] sites, the trivalent and divalent cations are randomly distributed. In the intermediate spinel there are number of unequal cations are present at the octahedral [B] sites [16].

1.6. Manganese ferrite

Manganese ferrite has been utilized as a part of numerous applications in different fields such as biomedical applications (hyperthermia treatments and drug delivery at particular site), industry purposes which comprising magnetic materials in scale down devices (photomagnetic materials, and magnetic storage devices) and the other are gas sensor and absorbent material for hot-gas. This applications are sensitive to their size which is mostly. Manganese Ferrite ($MnFe_2O_4$) is a magnetic material which crystallize in the spinel structure (AB_2O_4) with two divalent cation sites that contain 8 tetrahedral [A] sites and 16 octahedral [B] sites. The manganese ferrite nanoparticles properties are highly depends on the morphology, composition, and size of the material that is strongly related by the preparation conditions.

1.7. Effect of sintering temperature on manganese ferrite

Magnetic properties of material such as manganese ferrite depends on the sintering temperature as it which directly affects the saturation magnetization of the material. Hysteresis loops of $MnFe_2O_4$ nanoparticles annealed at different temperatures are shown in figure 1.7 [17].

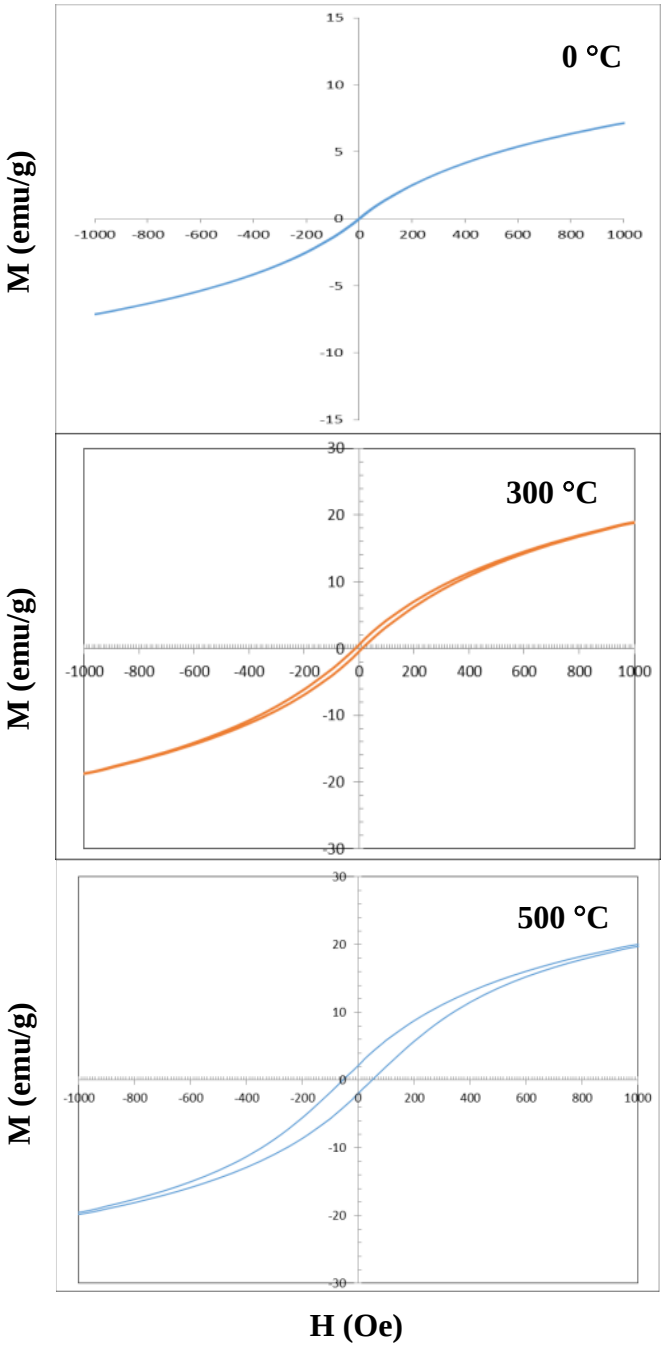

Figure 1.7. Hysteresis loops of $MnFe_2O_4$ annealed at 0 °C, 300 °C and 500 °C [26].

It was observed that nanoparticles are superparamagnetic when annealing at 0 ^{0}C in figure 1.7. Nanoparticles show ferromagnetic behaviour when annealed at 300 ^{0}C or at 500 ^{0}C. The magnetic properties (M_s, H_c, M_r, and M_r/M_s) are summarized in table 1.

Table 1.1. Magnetic parameters of $MnFe_2O_4$ nanoparticles [17].

Sample	**Hc (Gauss)**	**Ms (emu/gm)**	**Mr (emu/gm)**	**Mr/Ms**
$MnFe_2O_4$ at 0 °C	-	7	-	-
$MnFe_2O_4$ at 300 °C	13.92	38.60	0.5048	0.0131
$MnFe_2O_4$ at 500 °C	50	35.25	2.696	0.0764

The saturation magnetization value is lesser than the bulk $MnFe_2O_4$ which is reported as 80 emu/g [18]. This decrease in magnetization value is due to the presence of surface effects in the nanoparticles. The surface effect is due to the existence of disordered layer or called as inactive magnetic layer on the surface of the nanoparticles and also due to the rate of calcinations temperature [17]. By removing the magnetic field the direction of magnetization reorients to its adjacent axis magnetization direction that is named as the remanent ratio (Mr/Ms) [17]. The nature of the material is isotropic which is due to low value of remanent ratio of the prepared samples [19].

CHAPTER 2 LITRATURE REVIEW

The Synthesis and characterization of nano sized magnetic materials have arisen as an interesting topic of research from the last several years. There are many techniques to synthesize these magnetic nanoparticles ($MnFe_2O_4$) such as co-precipitation [20], thermal decomposition [21], reverse micelle [20,22], sol-gel method [23,24], ball milling [25,26,27], solid-phase reaction [28], pulsed laser decomposition [29], thermally activated solid state reaction [30] etc.

Chen et al. [1995] prepared fine particles of manganese ferrite in the size range of 5–15 nm by an aqueous co-precipitation method in which the digestion of nanoparticles were achieved at 100°C for the time 90 min in which the Curie temperature decreases with reducing the particle size particularly below to 10 nm. The finite size scaling is consistent with the decrease [5].

Chinnasamy et al. [2007] synthesized $MnFe_2O_4$ nanoparticles by co-precipitation method. The size is about 4 to 50 nm. The spinel ferrite structure is obtained from X-ray diffractograms of all samples. The higher value of Néel temperature is found to be 400 °C than the bulk $MnFe_2O_4$ which is 300 °C, this is due to the change of cations distribution among the tetrahedral [A] and octahedral [B] sites of the spinel lattice [31].

Mozaffari et al. [2008] prepared Manganese ferrite nano powders by co-precipitation method. Mean particle size was 5 nm that was obtained by Scherrer's formula. The saturation magnetization of the manganese ferrite nano powders results is 54.2 emu/g, which is less than the saturation magnetization of bulk manganese ferrite (80 emu/g) as reported [32].

Goodarz Naseri et al. [2011] prepared manganese ferrite nanoparticles which have cubic structure. These nanoparticles were calcinated at various temperatures from 723 to 873 K that are synthesized by a thermal treatment method. The average particle sizes were increased from 12 to 22 nm nanoparticles with the increase in calcination temperature as mentioned. These particles exhibits superparamagnetism nature because the saturation magnetization increases from 3 to 15.78 emu/g by the increasing in calcination temperature [33].

Elahi et al. [2011] have prepared manganese ferrite powder by a chemical co-precipitation method. The calcination was performed at 600 °C for 5 h. The value of crystallite size is calculated as 23.53 nm. Nanoparticles exhibits typical ferromagnetic behaviour, having a non-zero coercivity and remanence. The value of saturation magnetization is 16.36 emu/g [34].

Deraz et al. [2012] have synthesized manganese ferrite nanoparticles by combustion route. $MnFe_2O_4$ is obtained as single phase with the unequal shape. The size and crystallinity of nanoparticles were found to be strongly depending on both the remanent magnetization and the saturation magnetization [35].

Yasir Rafique et al. [2013] prepared highly dispersive nano spheres of $MnFe_2O_4$ by free hydrothermal method. The reaction temperature 140 °C to 220 °C is used for the sample preparation. The average diameter of the nanospheres is 47.3 nm with narrow size distribution, and average crystallite size about 22 nm with good crystallinity. The nanoparticles of $MnFe_2O_4$ have low coercivity, high saturation magnetization, and low remanence at 300 K as compared to reported nanoparticles. The closely shows superparamagnetic behaviour which is due to the close diameter of the prepared nanoparticles to the diameter for superparamagnetism [4].

Sharma et al. [2014] have synthesized nanoparticles of manganese ferrite by chemical co-precipitation method. They improved magnetic properties of $MnFe_2O_4$ nanoparticles with the help of annealing. The behaviour of these nanoparticles change from super paramagnetic to ferromagnetic upon annealing. The value of saturation magnetization is low as compared to bulk $MnFe_2O_4$ [17].

Ahalya et al. [2014] have synthesized manganese ferrite nanoparticles by a co-precipitation method. Nanoparticles were annealed at 300 ^{0}C, 600 ^{0}C and 900 ^{0}C for 4 h. By increasing the annealing temperature particle size increases with improved crystallinity [45].

Rao et al. [1997] prepared $Ni_{0.65}\,Zn_{0.35}\,Fe_20_4$ nanoparticles and sintered them at 1150 - 1300° C for 1 to 4 h. The XRD confirms single phase structure in all the samples [37].

Bhuiyan et al. [2010] prepared nanosized $NiFe_2O_4$ by solid state reaction. The XRD patterns approve that it is a single phase inverse spinel structure of the sample and the SEM micrographs shows that with the increase in sintering temperature the grain size increases [38].

Islam et al. [2012] prepared $Ni_{0.55}Zn_{0.45}Fe_2O_4$ by conventional double sintering ceramic technique. The X-ray diffraction pattern approve the samples to be a single phase cubic spinel structure. The Curie temperatures is found to be 321°C ± 1°C of the samples at various sintering temperatures. The Curie temperature of nanoparticles sintered at 1300 ˚C show significant enhancements which could be described from the fact that the zinc gets evaporated from the surface layer [39].

From this literature summary, it was found that the correlation between sintering temperature, magnetic and structural properties of $MnFe_2O_4$ magnetic nanoparticles is not well established. This dissertation is aimed to understand the effect of sintering temperature on magnetic and structural properties of $MnFe_2O_4$ nanoparticles synthesized by chemical co-precipitation method.

CHAPTER 3 SYNTHESIS AND CHARACTERIZATION

3.1. Synthesis of manganese ferrite nanoparticles

Materials: For the synthesis of manganese ferrite nanoparticles, the chemicals which are used Manganese (II) chloride tetra-hydrate ($MnCl_2.4H_2O$), ferric chloride hexa-hydrate ($FeCl_3.6H_2O$) and sodium hydroxide (NaOH), acetone which was purchased from Merck India. The Milli-Q ultrapure water is used to prepare all the aqueous solutions.

Method: Manganese ferrite nanoparticles were made by co-precipitation method using manganese (II) chloride tetra-hydrate ($MnCl_2.4H_2O$) and ferric chloride hexa-hydrate ($FeCl_3.6H_2O$). Protocols for the synthesis of $MnFe_2O_4$ nanoparticles are described in figure 3.1. In this method use sodium hydroxide (NaOH) as a base solution. Dissolve 10 mM of manganese (II) chloride tetra-hydrate (1.97g) in 200 mL Milli-Q ultrapure water. Dissolve 20 mM ferric chloride hexa-hydrate (5.4g) in 100 mL Milli-Q ultrapure water. 80 mM of sodium hydroxide solution (3.2g) in 150 mL Milli-Q ultrapure water was also prepared. When both acidic solutions get mixed. Add this acidic solutions into the prepared basic solution of Sodium hydroxide (NaOH) slowly. To maintain the pH of Acid + Basic solution at 10.50, we start adding dilute NaOH drop wise with the help of pipette. The reaction was allowable to continue for 20 min under a constant mechanical stirring. At that time, we got metal hydroxides. Now heat the sample at 90 ˚C for 6 hrs. Colloid is then cooled to room temperature and nanoparticles are decanted with the help of a magnet and washed with slightly warm Milli-Q ultrapure water 3-4 times. After washed with acetone and dried it overnight at 90 °C in oven. Therefore, grind the sample with the help of mortar pestle.

The following reaction took place:

10 mM $MnCl_2.4H_2O$ + 20 mM $FeCl_3.6H_2O$ + 80 mM NaOH $\longrightarrow$ 10 mM $MnFe_2O_4$ + 80 mM NaCl + 20 mM H_2O

As synthesized $MnFe_2O_4$ nanoparticles were annealed at 400 °C, 600 ˚C, and 900 ˚C for 8 hrs. (Figure 3.1)

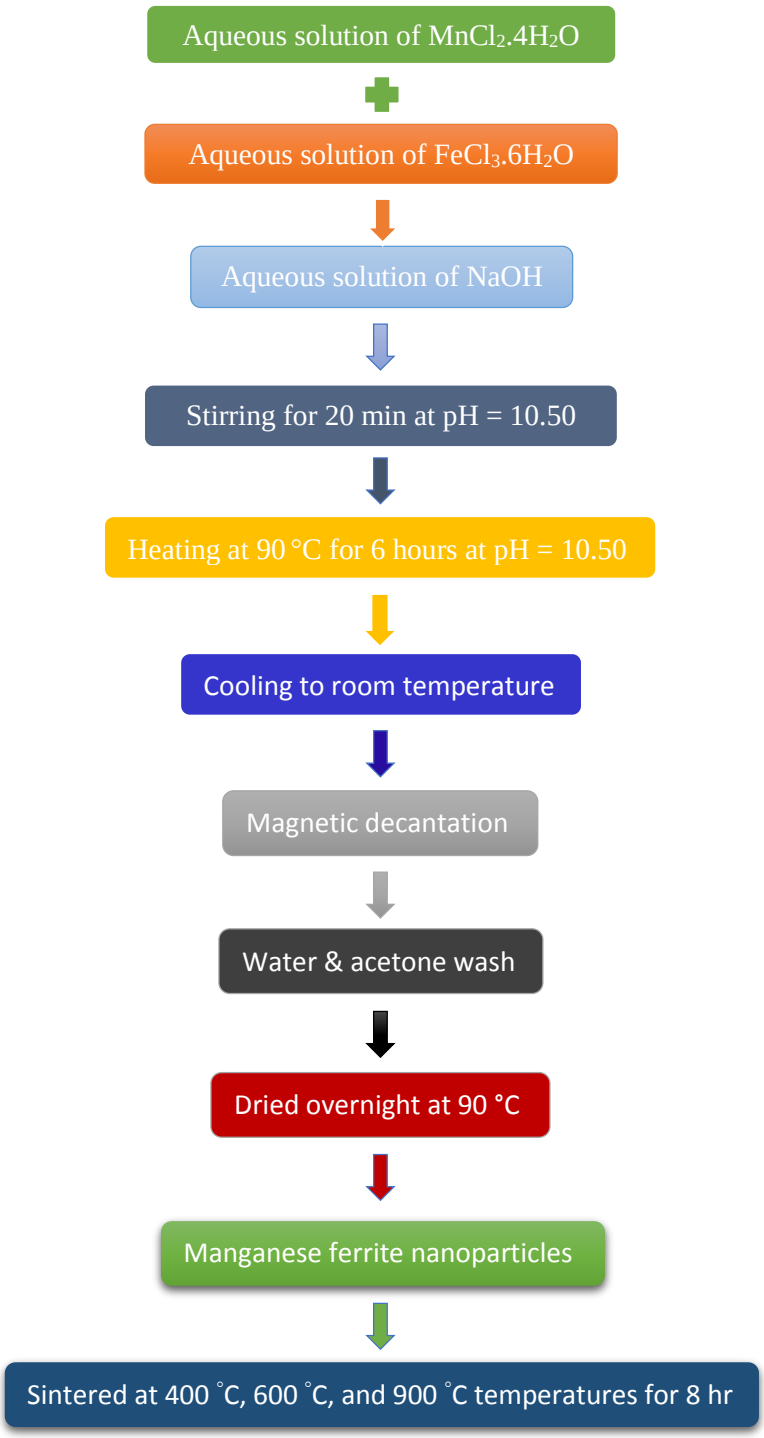

Figure 3.1. Protocols for the synthesis of $MnFe_2O_4$ nanoparticles.

3.2 Characterization

Crystalline size and structure of the $MnFe_2O_4$ nanoparticles are determined with the help of X-Ray Diffraction technique. The coercivity field (Hc), saturation magnetization (Ms), and

remanent magnetization (M_r) which are termed as magnetic properties are examined by Vibrating Sample Magnetometer (VSM). The hydrodynamic or particle size are examined with the help of Dynamic light scattering technique (DLS).

3.2.1 X-Ray Diffraction (XRD)

For the crystalline materials X-ray diffraction is a non-destructive method for characterization. This technique is used to determine the structure of crystalline material, preferred crystal orientation, phase, and other structural factors, such as strain, average grain size, crystal defects, crystallinity, and atomic spacing. The XRD analysis is based on the constructive interference of X-rays made of monochromatic light beam which are diffracted at definite angles in a crystalline sample from lattice planes. X-rays are like other electromagnetic rays that could be diffracted [40].

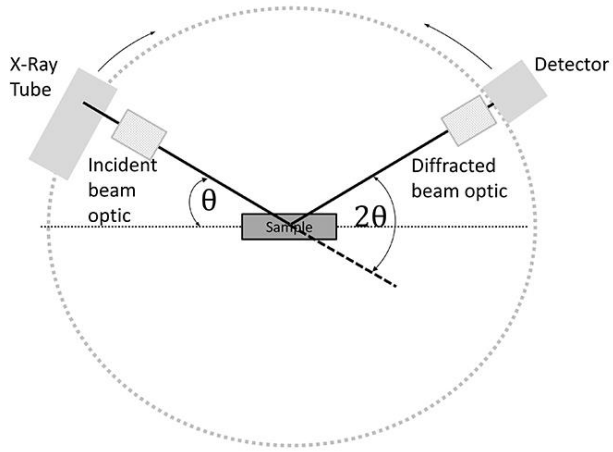

Figure 3.2. Schematic diagram of X-ray Diffraction experiment.

X-rays are produced by a cathode ray tube which further gets filtered to get a monochromatic beam and then focused towards the prepared sample. To attack target material with electrons, pick up the speed of the electrons in the direction of the target is by the applying voltage. When electrons have adequate energy to emit electrons from inner core shell of the target material then the X-rays are formed.

To determine the crystallite size Debye-scherrer method is used

$$d = \frac{k\lambda}{\beta cos\theta}$$

Where wavelength of X-rays is denoted by λ, Scherrer constant by k, angle of diffraction by θ, FWHM of highest intense peak are represented by β, and d is the crystallite size of nanoparticles [20]. The interplanar spacing can be determined from Bragg's law.

$$2dsin\theta = n\lambda$$

Where, Interplanar spacing is denoted by d, diffraction angle by θ, wavelength of incident X-rays by λ and order of diffraction by n. The schematic representation of X-ray diffraction from set of lattice planes is shown in figure 3.3

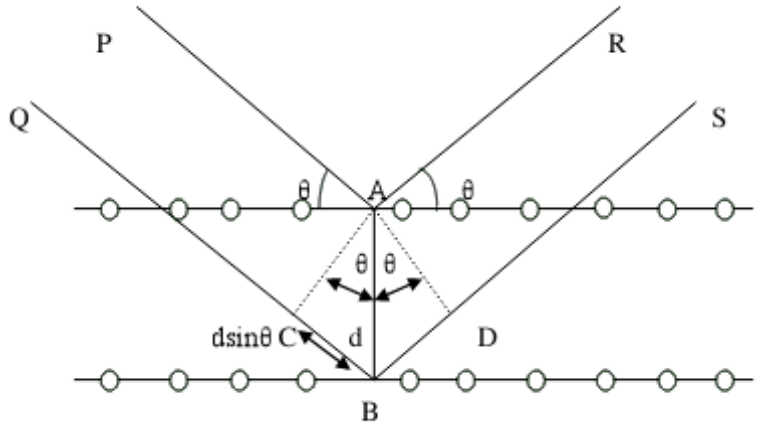

Figure 3.3. Schematic diagram of lattice planes in X-ray diffraction.

3.2.2 Vibrating Sample Magnetometer

VSM is a technical device which measures the sample magnetic properties. This technique is totally constructed on the Faraday's law which expresses that when there is a change in flux, an electromagnetic force is induced in the coil. With the change in magnetic field, electric field produced. A magnetic sample in the VSM setup (Figure 3.4), is moving in proximity of two pickup curls.

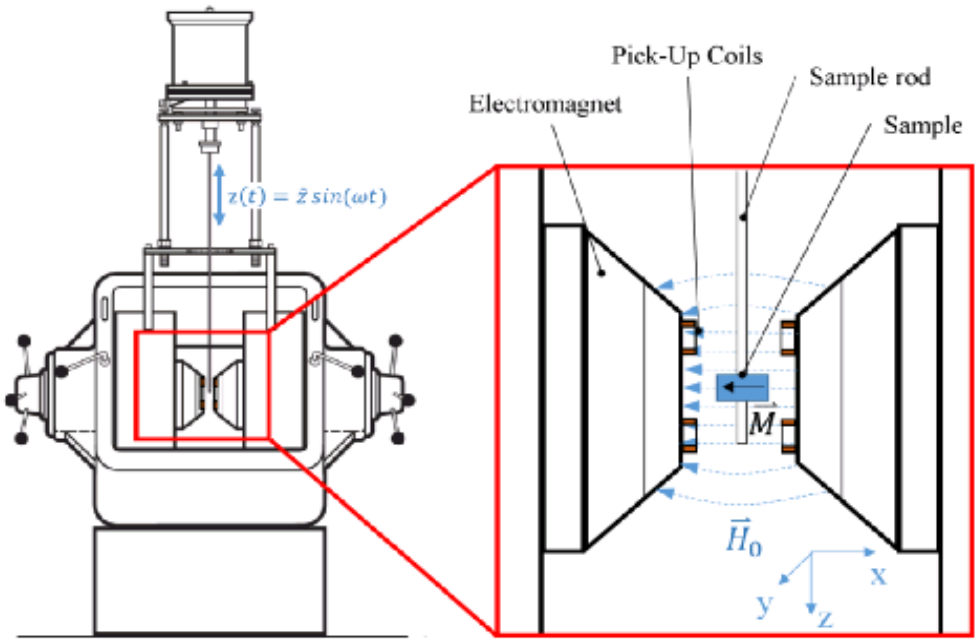

Figure 3.4. Schematic diagram of vibrating sample magnetometer.

The sample is kept at a constant magnetic field. The magnetic domains of the sample gets magnetized and aligned with the presence of constant applied field. Larger value of magnetization results as corresponding to strong constant field. The sample is positioned in a constant magnetic field (H) and the magnetic moment (emu) will be induced in the sample by mechanically vibrating sample in between the sensing curls due to applied field. The magnetic moment will generate a magnetic field nearby the sample. The sample magnetic properties is determined from the M-H curve like remanent magnetization (Mr), saturation magnetization (Ms), and the coercivity (Hc).

3.2.3. Dynamic light scattering (DLS)

Dynamic light scattering (DLS) is a technique in physics that has become a powerful light-scattering technique for learning the properties of suspensions and solutions of colloids, polymers and macromolecules. The basic principle of dynamic light scattering is that when the specimen is irradiated by the laser beam, the variations of the dispersed light are noticed at a known scattering angle θ by a detector known as fast photon detector. Photon correlation spectroscopy is centred on the statistical analysis of light scattering intensity variations arising

from the Brownian diffusion of particles in a controlled environment (temperature, viscosity, refractive index). The rate of the Brownian motion is demarcated by the translational diffusion coefficient (D) which is given as

$$D = 1/\tau q^2$$

Where τ is the delay time, q is the wave vector. By using the Stokes-Einstein relation or equation we can convert the translational diffusion coefficient into a particle size [51].

Figure 3.5. Photographic view of Dynamic light scattering setup (90 Plus particle size analyzer from Brookhaven Instruments).

$$d = k_B T/3\pi D\eta_o$$

Where, D is the diffusion constant, T is the temperature, η_o is the viscosity of solvent and d is the particles hydrodynamic diameter which is defined as the diameter that a particle would have in order to diffuse at the same rate as the particle being measured [41].

CHAPTER 4 RESULTS AND DISCUSSIONS

4.1. X-Ray Diffraction

Manganese ferrite nanoparticles are prepared with the co-precipitation technique. As synthesized nanoparticles are 400 °C, 600 °C, and 900 °C. Each sample is subject to powder X-ray diffraction. From X-ray diffraction crystallite size and crystal structure have been determined. The range from $20° \leq 2\theta \leq 80°$ was used to collect from the X-ray diffraction data at room temperature. CuKα monochromatic radiation which having wavelength about 1.54 Å was used in XRD. [12].

The crystallite size was found from the highest intense peak of the XRD pattern with the help of Scherrer formula i.e.

$$\boldsymbol{d = \frac{k\lambda}{\beta cos\theta}}$$

Where wavelength of X-rays is denoted by λ, angle of diffraction by θ, FWHM of highest intense peak by β is and, d is the crystallite size of nanoparticles [20]. Results are précised in the table 4.1.1.

Table 4.1.1. Crystallite Size of manganese ferrite nanoparticles sintered at different temperatures.

Sintering temperature (˚C)	Crystallite Size (nm)
25	18
400	16
600	11
900	19

The XRD pattern of $MnFe_2O_4$ as-synthesized nanoparticles is shown in figure 4.1.1. Each diffraction peak is index well with the inverse spinel structure of $MnFe_2O_4$ with the Fd3m space group. The pattern matches well with the JCPDS card No. 01-088-1965 Jacobsite syn. Which is the mineral of manganese ferrite. Peaks corresponding to any other crystallographic phase is

absent indicating that as synthesized nanoparticles. Crystallizes into single phase inverse spinel structure. The broadening in crystallite size is due to the small size of nanoparticles. The lattice parameters are as a = b = c = 8.4970 Å and $\alpha = \beta = \Upsilon = 90°$.

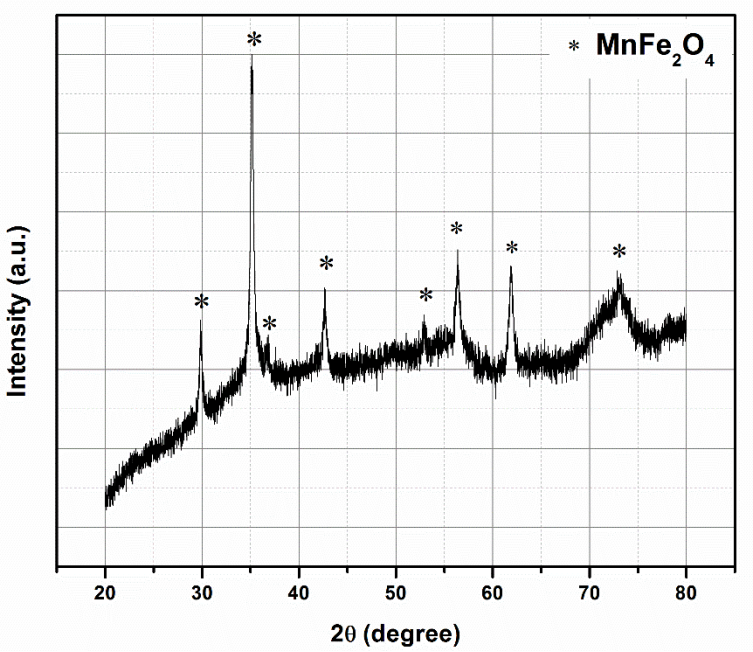

Figure 4.1.1. X-ray diffraction pattern of $MnFe_2O_4$ nanoparticles sintered at 25 °C.

XRD pattern of manganese ferrite nanoparticles sintered at 400 °C is shown in figure 4.1.2. This pattern does not matches with the JCPDS card No. 01-088-1965 which indicating that nanoparticles have under gone phase transformation.

All peaks of the sample are related to a cubic multi-phase spinel structure with the Fd3m space group matching with the JCPDS card No. 00-013-0162 with an empirical formula Mn_3O_4 and JCPDS card No. 00-039-1346 with an empirical formula Υ-Fe_2O_3.

$$MnFe_2O_4 \xrightarrow{\Delta} \Upsilon\text{-}Fe_2O_3 + Mn_3O_4 \quad (\Delta = 400\ °C\ )$$

The average crystalline size of the sample was about to 16 nm calculated with the help of Scherer formula. The lattice parameters of the Mn_3O_4 are as a = b = c = 8.42 Å and $\alpha = \beta = \Upsilon = 90°$ and of Υ-Fe_2O_3 are as a = b = c = 8.35 Å and $\alpha = \beta = \Upsilon = 90°$.

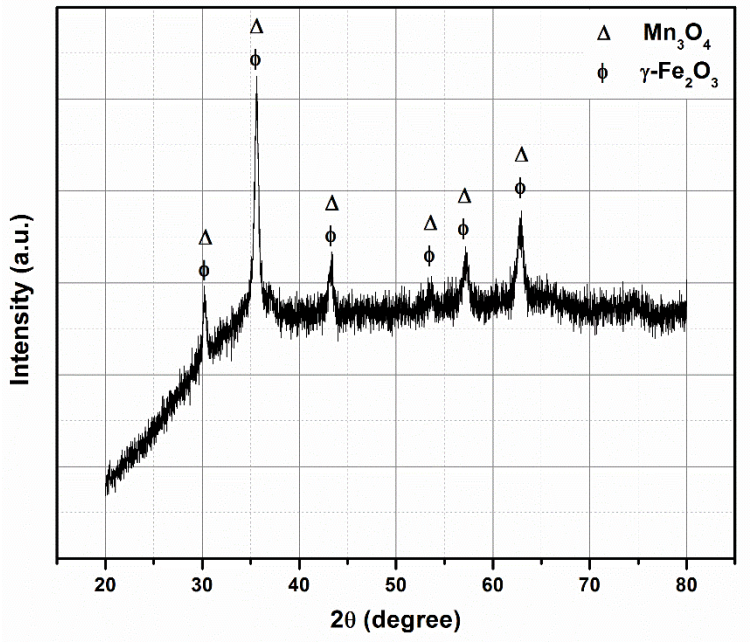

Figure 4.1.2. X-ray diffraction pattern of $MnFe_2O_4$ nano particles sintered at 400 ° C.

XRD pattern of manganese ferrite nanoparticles after sintering at 600 °C is shown in figure 4.1.3. It also shows multi-phase structure. The pattern matches with two crystallographic phases. One of them is with the cubic phase with spinel structure with the space group of Fd3m. It is worthy agreement with JCPDS card No. 00-013-0162 of Mn_3O_4. The other phase is rhombohedral phase with the R-3c space group. It matches with JCPDS card No. 00-089-8103 of α-Fe_2O_3. This means that as the sintering temperature is raised to 600 °C the Υ-Fe_2O_3 phase transforms to α-Fe_2O_3 phase.

$$\Upsilon\text{-}Fe_2O_3 + Mn_3O_4 \xrightarrow{\Delta} \alpha\text{-}Fe_2O_3 + Mn_3O_4 \quad (\Delta = 600\ °C)$$

The broadening of the peaks in the sintered manganese ferrite sample at 600 °C decreases. This might be due to the grain growth of the sample. The average crystalline size of the sample was about to 11 nm calculated with the help of Scherer formula. The lattice parameters of the Mn_3O_4

is a = b = c = 8.42 Å and α = β = ϒ = 90° and of α-Fe_2O_3 is a = b = 5.0206 Å, c = 13.7196 and α = β = 90°, ϒ = 120°.

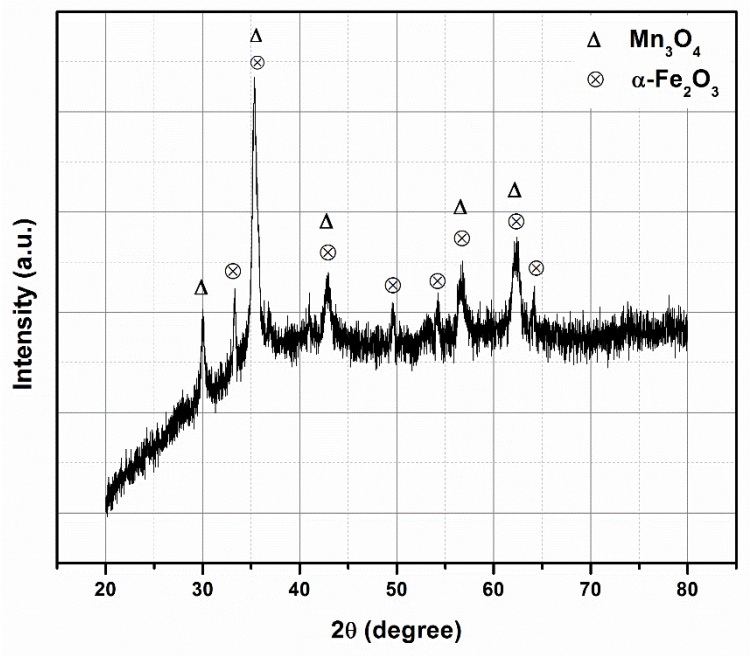

Figure 4.1.3. X-ray diffraction pattern of $MnFe_2O_4$ nano particles sintered at 600 ° C.

XRD pattern of manganese ferrite nanoparticles after sintering at 900 ˚C is shown in figure 4.1.4. The pattern matches with the crystallographic phases. One of them is the cubic phase with spinel structure with the la-3 space group. It matches with the JCPDS card No. 01-076-0076 of $FeMnO_4$. The second phase is the rhombohedral with the R-3c space group. It matches with JCPDS card No. 00-089-8103 of α-Fe_2O_3. The third phase again is a cubic phase with spinel structure with the Fd-3m space group. It matches with the phase JCPDS card No. 01-089-8103 of Fe_3O_4.

α-Fe_2O_3 + Mn_3O_4 $\xrightarrow{\Delta}$ $FeMnO_3$ + α-Fe_2O_3 + Fe_3O_4 (Δ = 900 °C)

The broadening of the peaks after sintering 900 °C further decreases. The average crystalline size of the sample was 19 nm. The lattice parameters of the $FeMnO_3$ is a = b = c = 9.36 Å, α = β = ϒ = 90° and of α-Fe_2O_3 is a = b = 5.02 A°, c = 13.71 Å, α = β = 90°, ϒ = 120° and of β-Fe_3O_4 is a = b = c = 8.4910 Å, α = β = 90°.

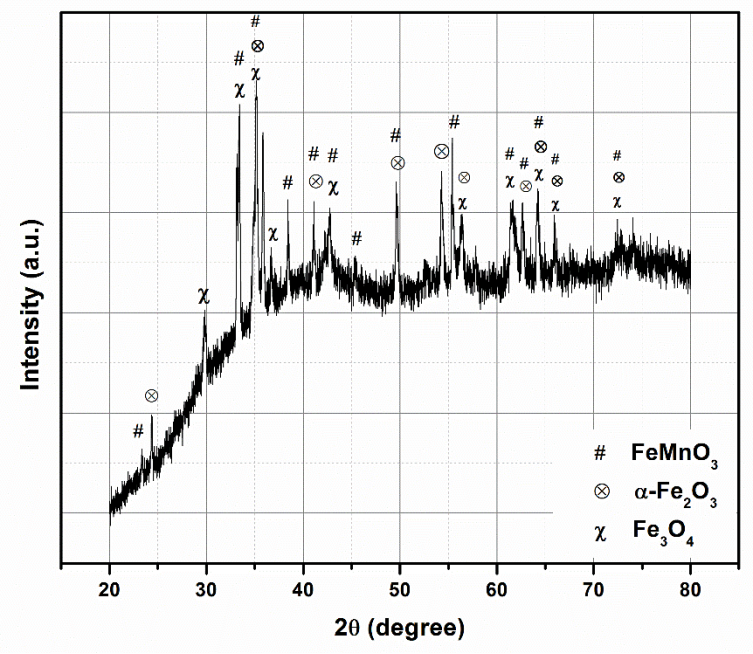

Figure 4.1.4. X-ray diffraction pattern of $MnFe_2O_4$ nano particles sintered at 900 ° C.

4.2. Magnetic properties of $MnFe_2O_4$

Magnetic properties of the $MnFe_2O_4$ nanoparticles are characterized by using Lake Shore Vibrating Sample Magnetometer (VSM). Magnetic characteristics of nanoparticles like saturation magnetization strongly depend on the preparation method or technique and condition apply for synthesis. The M-H loop are measured up to 10 kOe field at room temperature.

The hysteresis loops of $MnFe_2O_4$ nanoparticles sintered at 25 °C, 400 °C, 600 °C and 900 °C are shown in figure 4.2.1. From the graph of Magnetization (M) versus applied Magnetic field (H) we concluded that all the samples displays superparamagnetic behaviour which means zero coercivity and zero remanence. Superparamagnetism is the form of magnetism that seems in small ferri or ferromagnetic nanoparticles. In these type of nanoparticles, magnetization arbitrarily flip their direction under the effect of temperature.

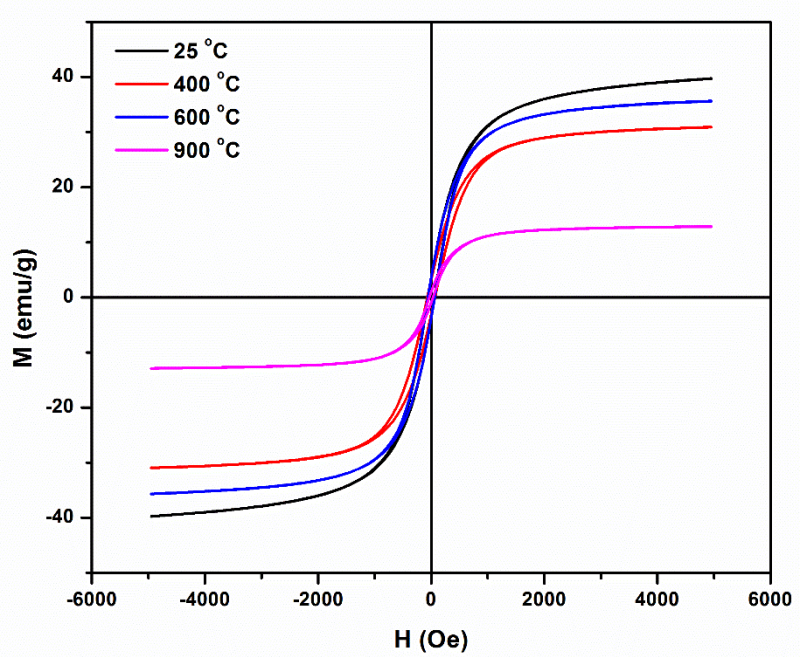

Figure 4.2.1. Magnetization curves of $MnFe_2O_4$ nanoparticles sintered at 25 °C, 400 °C, 600 °C and 900 °C.

The magnetization curve of superparamagnetism is an collection of isolated magnetic particles which could be expressed with the help of Langevin's theory with an norms i.e., particles have spherical shape, thermal energy have dominance over anisotropy energy, ($KV << k_BT$), where Boltzmann constant is denoted by k_B, absolute temperature by T, anisotropy constant by K and volume of the particles by V, polydispersed nature of particles which generally follows the log-normal distribution function and the average domain magnetization, M_d, of the particles which generally remains persistent with a given size distribution [40]. The distribution in particle size are seen in the case of interacting superparamagnetic particles, Magnetization could be written as;

$$M = M_s L(\alpha)$$

Where magnetization is termed as M, saturation magnetization is termed as M_s and here L (α) is the Langevin's function

$$L(\alpha) = coth(\alpha) - 1/\alpha$$

Where α is known as the Langevin's parameter and written as

$$\alpha = \mu H / k_B T$$

Where magnetic moment of the nanoparticles are termed as μ, applied field by H, Boltzmann constant by k_B and absolute temperature by T.

By fitting with Langevin's function, we got the value of saturation magnetization (M_s) and magnetic moment (μ) of all the four samples are determined. The results are mentioned in a table 4.2.1.

Table 4.2.1. Values of saturation magnetization (Ms) and magnetic moment (μ) of $MnFe_2O_4$ sintered at 25 °C, 400 °C, 600 °C, and 900 °C.

$MnFe_2O_4$ at (°C)	M_s (emu/g)	μ (μ_B)
25	40.7	20765
400	32.0	23237
600	36.6	24505
900	13.2	29881

The Magnetization (M) versus Magnetic field (H) with Langevin's theory of $MnFe_2O_4$ nanoparticles sintered at 25 °C, 400 °C, 600 °C, 900 °C are shown in figure 4.2.2.

The change of magnetization is also affected by the phases induced in the sample due to sintering. When the $MnFe_2O_4$ is at room temperature (25 °C) the magnetization is due to the presence of $MnFe_2O_4$ phase which has saturation magnetization of 54.2 emu/g as reported in previous paper by Mozaffari et al. in 2008. When it is sintered at 400 °C, magnetization decreases marginally due to the development of ϒ- Fe_2O_3.

As we further sintered at 600 °C there is a phase transformation of Fe_2O_3 from ϒ- Fe_2O_3 to α-Fe_2O_3. This transformation showed decrease the magnetization of the sample but we have observed a rise in magnetization from 30.53 emu/g to 35 emu/g. This may be because of compensation of decrease in magnetization due to α-Fe_2O_3 by enhancement in the phase fraction of Mn_3O_4. Further a sharp drop in the magnetization was observed when it was sintered at 900 °C.

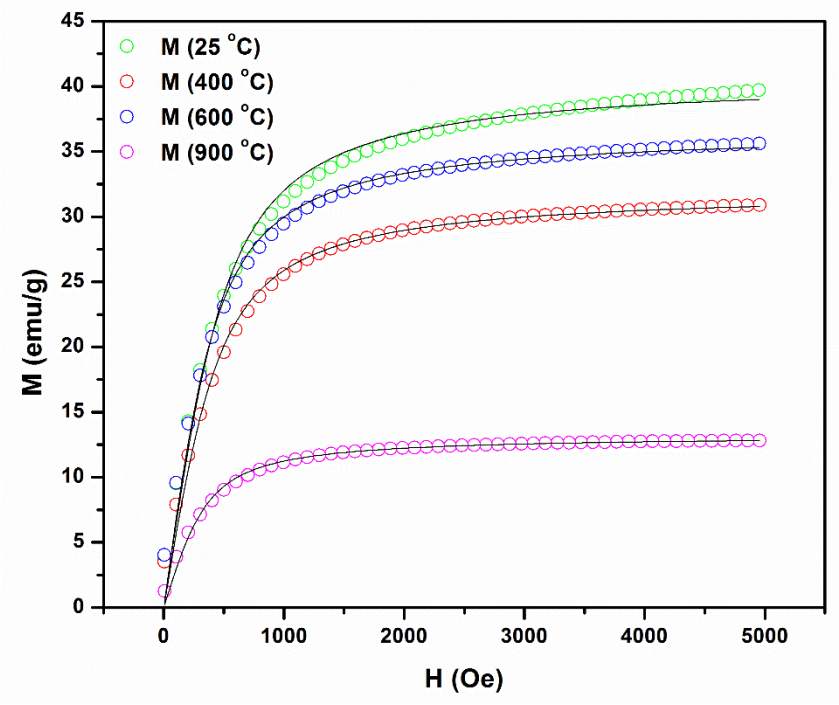

Figure 4.2.2. Magnetization (M) versus magnetic field (H) of $MnFe_2O_4$ nanoparticles sintered at 25 °C, 400 °C, 600 °C, and 900 °C fitted with Langevin's theory.

4.3. Dynamic light scattering (DLS)

Dynamic light scattering (DLS) is a light scattering technique which measures the Brownian motion of the particles and determine its hydrodynamic size. Brownian motion highly depends on the size of the particles. Bigger the size of the particles, gentler the Brownian motion and vice-versa. The size of the particle is deliberate from the translational diffusion coefficient by using the Stokes – Einstein relation or equation;

$$d = k_B T / 3\pi D\eta_o$$

Where, D is the diffusion constant, T is the temperature, η_o is the viscosity of solvent and d is the particles hydrodynamic diameter [41].

When there is distribution of sizes are present, the effective diameter measured is a mean diameter that is weighted by the intensity of light spread by each particle. Here, the effective Diameter represents an average size of the particles in the sample and the polydispersity is a measure of the non-uniformity's that exist in the particle size distribution, Avg. count rate is a measure of signal intensity [41]. Particle size and the polydispersity index of the $MnFe_2O_4$ at room temperature, 400 °C, 600 °C, and 900 °C are given below in table 4.3.1.

Table 4.3.1. Mean hydrodynamic diameter and polydispersity index of $MnFe_2O_4$ nanoparticles sintered at 25 °C, 400 °C, 600 °C, and 900 °C.

Sintering temperature (°C)	Mean hydrodynamic diameter (nm)	polydispersity index
25	66	0.329
400	88	0.289
600	88.06	0.256
900	97	0.354

The particle size histogram is fitted with lognormal particle size distribution function which is expressed as

$$P(D) = \frac{1}{(D\sigma\sqrt{2\pi})} exp\left[-\frac{\left(ln\left(\frac{D}{D0}\right)\right)^2}{2\sigma^2}\right]$$

Where D is the particle diameter, σ is the standard deviation, and ln D_0 is mean of ln D. The hydrodynamic size distribution fitted with log-normal distribution of $MnFe_2O_4$ nanoparticles sintered at 25 °C, 400 °C, 600 °C, and 900 °C are shown in figure 4.3.1. to 4.3.4.

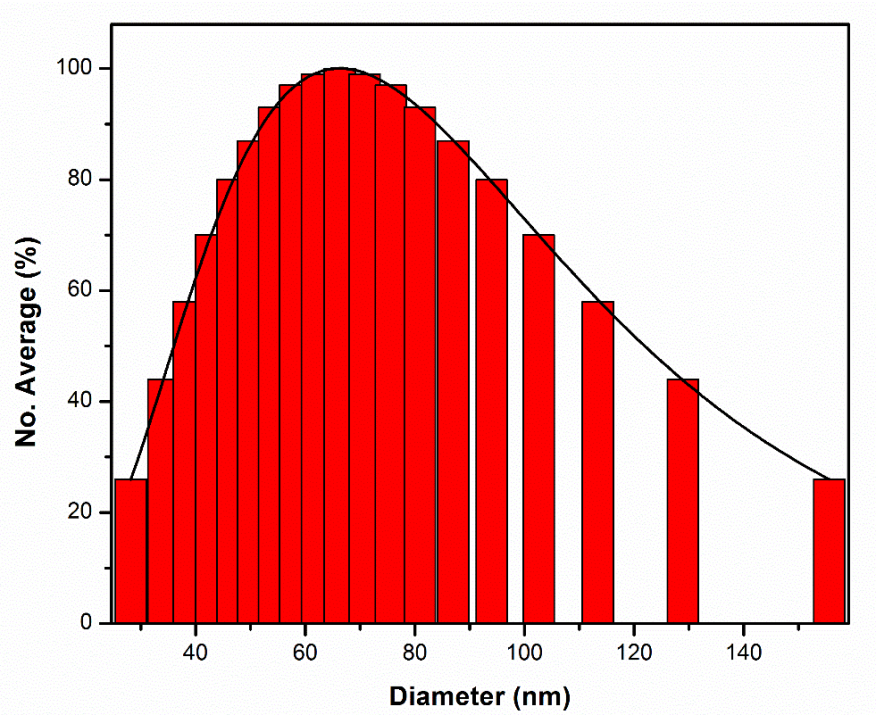

Figure 4.3.1. Hydrodynamic size distribution of $MnFe_2O_4$ nanoparticles sintered at 25 °C.

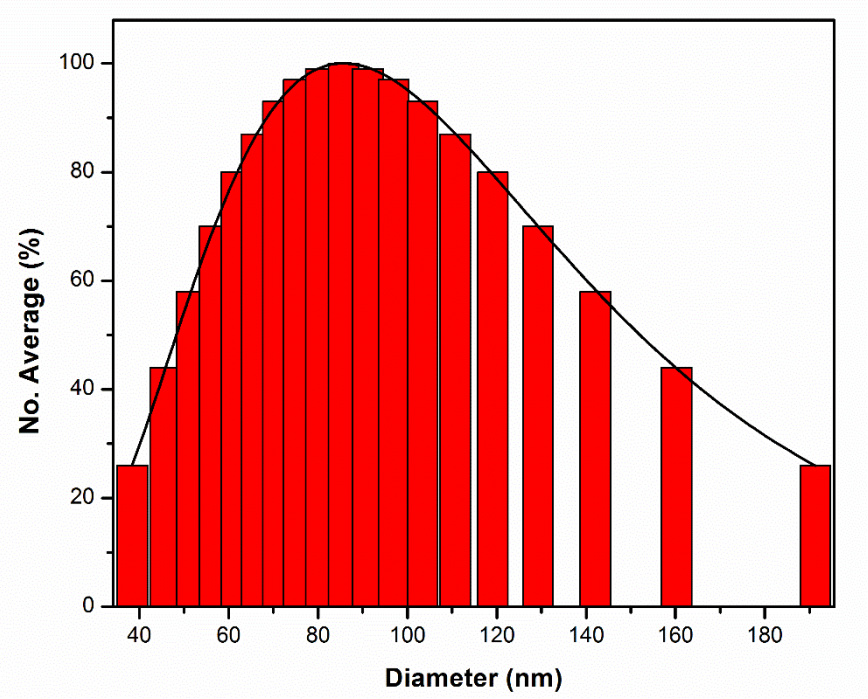

Figure 4.3.2. Hydrodynamic size distribution of $MnFe_2O_4$ nanoparticles sintered at 400 °C.

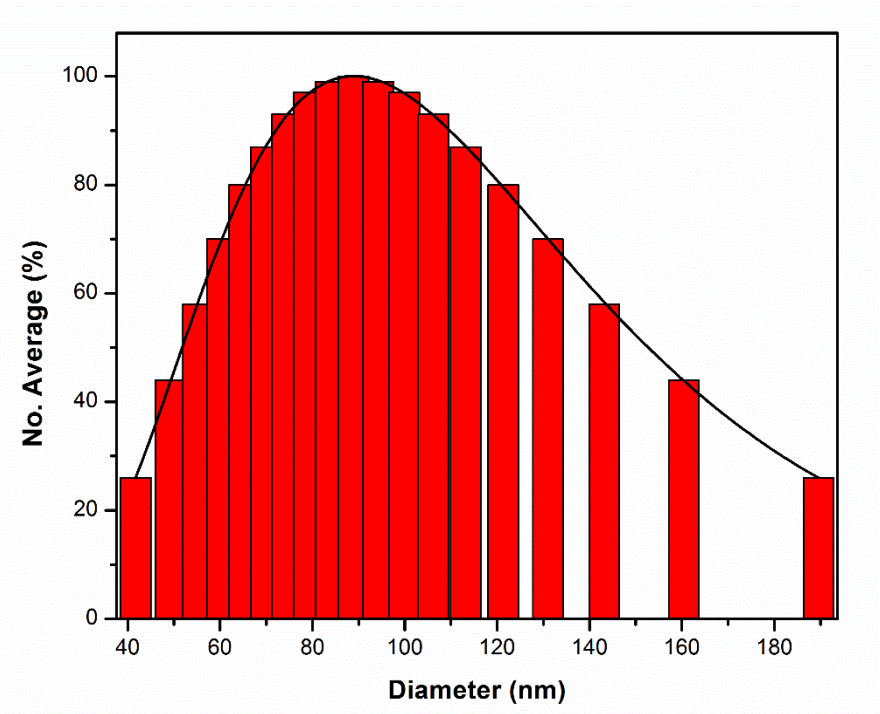

Figure 4.3.3. Hydrodynamic size distribution of $MnFe_2O_4$ nanoparticles sintered at 600 °C.

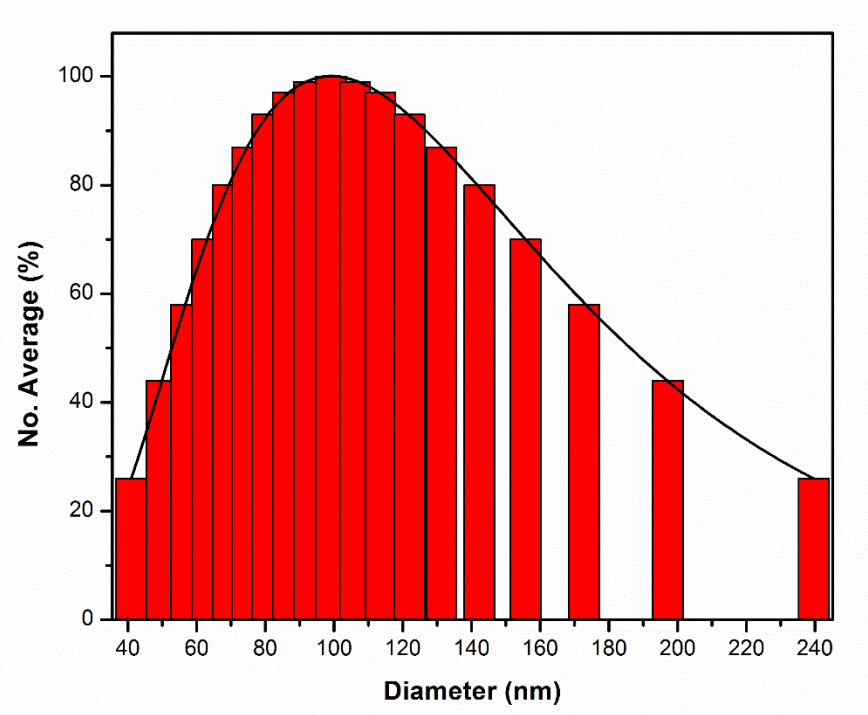

Figure 4.3.4. Hydrodynamic size distribution of $MnFe_2O_4$ nanoparticles sintered at 900 °C.

CHAPTER 5 CONCLUSIONS

$MnFe_2O_4$ nanoparticles are synthesized by co-precipitation method. As synthesized nanoparticles are superparamagnetic with the single phase inverse spinel structure. The structural and magnetic properties of these nanoparticles are strongly depend on the sintering temperature of the sample. The observed changes in magnetization value due to sintering is in good agreement with corresponding changes in its crystallographic phases as observed in X-ray diffraction studies. Upon sintering $MnFe_2O_4$ first transforms to Υ-Fe_2O_4 and Mn_3O_4 at 400 °C; then Υ-Fe_2O_4 phase is further transform to α-Fe_2O_3 at 600 °C. Further sintering will produce $FeMnO_3$, α-Fe_2O_4, and Fe_3O_4 phases at 900 °C.

REFERENCES

1. L. Filipponi, D. Sutherland, "*Nano science and Nanotechnologies" - A Brief Introduction* (2007)
2. N. Lane, *"Nano Research*", **3** (2005) 95
3. Masuo Hosokawa, Kiyoshi Nogi, Makio Naito, Toyokazu Yokoyama, "*Nanoparticle Technology Handbook* " First ed., Elsevier: Oxford (UK) 2007
4. M. Yasir Rafique, Pan Li-Qing, Qurat-ul-ain Javed, M. Zubair Iqbal, Qiu Hong-Mei, M. Hassan Farooq, Guo Zhen-Gang, and M. Tanveer, "*Chin. Phys. B*", **22** (2013) 107101(1-7)
5. J. P. Chen, C. M. Sorensen, K. J. Klabunde, G. C. Hadjipanayis, E. Devlin and A. Kostikas., *"Physical review",* **54** (1996) 9288-9296
6. M. Mozaffari, J. Amighian, E. Darsheshdar, *"Magnetism and Magnetic Materials"*, **350** (2014) 19.
7. M. Meshram, N. K. Agarwal, B. Sinha, P. S .Mishra, *"Magnetism and Magnetic Materials"*, **271** (2004) 207
8. A. B. Gadkari, T. J. Shinde, P. N. Vasambekar, *"Materials Chemistry and Physics"*, **114** (2009) 505
9. M. A. Ahmed, A. A. E. Khawlani, *"Magnetism and Magnetic Materials"*,**329** (2009) 1959
10. L. Kumar, P. Kumar, A. Narayan, M. Kar, *"International Nano Letters"*,**3** (2013) 8
11. M. Houshiar, F. Zebhi, Z. J. Razi, A. Alidoust, Z. Askari, *"Magnetism and Magnetic Materials"*, **371** (2014) 43
12. C. Fei, Y. Zhang, Z. Yang, Y. Liu, R. Xiong, J. Shi, X. Ruan, *"Magnetism and Magnetic Materials"*, **323** (2011) 1811
13. C. Liu, B. Zou, A. J. Rondinone, Z. J. Zhang, *"American Chemical Society"*, **122** (2000) 6263
14. I. Sharifi, H. Shokrollahi, M. M. Doroodmand, R. Safi, *"Magnetism and Magnetic Materials"*, **324** (2012) 1854
15. M. G. Naseri, E. B. Saion, H. A. Ahangar, A. H. Shaari, M. Hashim, *"Nanomaterials"*, DOI:10.1155/2010/907686
16. A. Franco, V. Zapf, *"Magnetism and Magnetic Materials"*, **320** (2008) 709
17. Uma Shankar Sharma, Ram Naresh Sharma and Rashmi Shah, *"Int. Journal of Engineering Research and Applications"* **4** (2014) 14-17

18. P. J. Van der Zaag, A. Noordermeer, M. T. Johnson and P. E. Bongers, "*Phys. Rev. Lett"*., **68** (1992) 3112.
19. Toksha B.G., Sagar E. Shirsath, S.M. Patange, K.M.Jadhav, "*Solid State Commun",* **147** (2008) 479–483.
20. Adam J R, Chao L and Zhang Z, *" J. Phys. Chem. B"*, **105** 2001 7967
21. Balaji G, Gajbhiye N S, Wilde G and Weissmuller, *"J. Magn. Magn. Mater."* **242** (2002) 617
22. Liu C, Zou B S, Rondinone A J and Zhang Z, " *J. Phys. Chem. B*" **104** (2000) 1141
23. Nemoto N, Schleich DM, Zhang Y, *"Mater. Res. Bull",* **30** (1995) 447-452.
24. Gajbhiye NS, Balaji G, *"Thermochemical Acta."* **385** (2002) 143-151.
25. Mahmoud MH, Hamdeh HH, Ho JC, O'Shea MJ, Walker JC*, "J. Magn. Magn. Mater."* **220** (2000) 139-146.
26. Muroi M, Street R, McCormick PG, Amighian, *"Physical Review B.,"***63** (2001) 184414.
27. Ding J, Street R, McCormick PG, and *"J. Magn. Magn. Mater."* **171** (1997) 309-314.
28. Deraz NM, El-Shobaky GA, *"Thermochemical Acta."* **375** (2001) 137-145.
29. Mahmoud MH, Williams CM, Cai J, Siu I, Walker JC, *"J. Magn. Magn. Mater."* **261** (2003) 314-318.
30. Alvani C, Ennas G, La Barbera A, Marongiu G, Padella F, Varsano F, *"Int. J. Hydrogen Energy"* **30** (2005) 1407-1411.
31. C. N. Chinnasamy, Aria Yang, S. D. Yoon, Kailin Hsu, M. D. Shultz, E. E. Carpenter, S. Mukerjee, C. Vittoria, V. G. Harris*, " Journal of applied physics"* **101** (2007) 09M509
32. Mortaza Mozaffari, Behshid Behdadfar, Jamshid Amighian, *"Iranian Journal of Pharmaceutical Sciences"*, **4** (2008) 115-118
33. M. GoodarzNaseri, E.BinSaion, H.AbbastabarAhangar, M.Hashim, A.H.Shaari, *"Journal of Magnetism and Magnetic Materials"*, **323** (2011) 1745–1749
34. Irfan Elahi, Rabab Zahira, Kiran Mehmood, Arifa Jamil and Nasir Amin, *"African Journal of Pure and Applied Chemistry"*, **6** (2012) 1-5
35. N. M. Deraz, A. Alarifi, *"Int. J. Electrochem. Sci."* , **7** (2012) 5534 – 5543
36. K. Ahalya, N.Suriyanarayanan, S.Sangeetha, *"Materials Science in Semiconductor Processing"*, **27** (2014) 672–681
37. B. Parvatheeswara Rao, P. Subba Rao, K. Rao, *"Journal de Physique IV Colloque"*, **07** (1997) 241-242
38. Mahabub Alam Bhuiyan, Sheikh Manjura Hoque Heikh and Shamima Choudhury, *"Journal of Bangladesh Academy of Sciences",* **34** (2010) 189-195,

39. Robiul Islam, Md Obaidur Rahman1, M. Abdul Hakim, Dilip Kumar Saha, Saiduzzaman, Saroaut Noor, Md Al-Mamun, *"Materials Sciences and Applications"*, **3** (2012) 326-331
40. Rucha Desai, Vipul Davariya, Kinnari Parekh and Ramesh V Upadhyay, Pramana *"Journal of Physics.",* **73** (2009) 765-780
41. Instruction Manual for 90 plus Multi Angle Particle Sizing Option operational Manual by Brookhaven Instruments Corporation, New York, USA